Radiology

ORIGINAL RESEARCH · NEURORADIOLOGY

Identification of Biological Subtypes of Friedreich Ataxia with Structural MRI-based Machine Learning

Giuseppe Pontillo, MD, PhD[1,2,3,4] • *Simone Penna, MSc*[5] • *Filippo Arrigoni, MD, PhD*[6] • *Benjamin Bender, MD*[7] • *Sylvia Boesch, MD*[8] • *Arturo Brunetti, MD*[1] • *Fernando Cendes, MD, PhD*[9,10] • *Sidhant Chopra, PhD*[11] • *Louise A. Corben, PhD*[12,13] • *Andreas Deistung, PhD*[14] • *Martin B. Delatycki, PhD*[12,13,15] • *Stefano Diciotti, PhD*[16] • *Imis Dogan, PhD*[17,18] • *Gary F. Egan, PhD*[19] • *Marcondes C. França Jr, MD, PhD*[9,10] • *Nellie Georgiou-Karistianis, PhD*[20] • *Sophia L. Göricke, MD*[21] • *Pierre-Gilles Henry, PhD*[22] • *Carlos R. Hernandez-Castillo, PhD*[23] • *Diane Hutter, RN*[22] • *James M. Joers, PhD*[22] • *Christophe Lenglet, PhD*[22] • *Tobias Lindig, MD*[7] • *Raffaele Lodi, MD, PhD*[24,25] • *David N. Manners, PhD*[25,26] • *Alberto R. M. Martinez, MD, PhD*[9,10] • *Andrea Martinuzzi, MD, PhD*[27] • *Chiara Marzi, PhD*[28] • *Mario Mascalchi, MD, PhD*[29] • *Wolfgang Nachbauer, MD, PhD*[8] • *Chiara Pane, MD, PhD*[30] • *Denis Peruzzo, PhD*[6] • *Pramod K. Pisharady, PhD*[22] • *Kathrin Reetz, MD*[17,18] • *Thiago J. R. Rezende, PhD*[9,10] • *Sandro Romanzetti, PhD*[17,18] • *Francesco Saccà, MD, PhD*[31] • *Ludger Schoels, MD*[32,33] • *Jorg B. Schulz, MD*[17,18] • *Ambra Stefani, MD, PhD*[8] • *Matthis Synofzik, MD, PhD*[32,33] • *Sophia I. Thomopoulos, BA*[34] • *Paul M. Thompson, PhD*[34] • *Dagmar Timmann, MD*[35] • *Caterina Tonon, MD, PhD*[24,25] • *Marinela Vavla, MD, PhD*[27,36] • *Ian H. Harding, PhD***[37,38] • *Sirio Cocozza, MD, PhD***[1]

** I.H.H. and S.C. are co–senior authors.

Author affiliations, funding, and conflicts of interest are listed at the end of this article.

Radiology 2026; 318(3):e251386 • https://doi.org/10.1148/radiol.251386 • Content codes: NR MR AI

Background: Friedreich ataxia (FRDA) is an inherited, progressive neurodegenerative disease. Interindividual heterogeneity in the rate and phenotypic profile of disease progression indicates a biologic variability in the pattern and spatial evolution of underlying changes, but the occurrence of possible FRDA subgroups, which could aid in clinical trial design and treatment, are still unknown.

Purpose: To obtain a structural MRI–based stratification of participants with FRDA using the Subtype and Stage Inference (SuStaIn) algorithm and determine whether these subgroups are biologically meaningful and clinically relevant.

Materials and Methods: This multicenter secondary analysis of prospectively acquired data included structural MRI and clinical-demographic data from participants from the ENIGMA-Ataxia working group. MRI biomarkers were analyzed using the SuStaIn algorithm to identify subgroups with distinct patterns and disease stages. The clinical and genetic relevance of these subgroups were assessed within a linear model framework.

Results: This study included 565 participants (mean age, 32 years ± 13.1 [SD]; 286 women; 275 participants with FRDA and 290 healthy controls). SuStaIn identified three subtypes: *(a)* a classical subtype (66.5% [183 of 275 participants]), characterized by an ascending gradient of damage from brainstem to cerebellar cortex to cerebrum; *(b)* an early cerebral subtype (25.8% [71 of 275 participants]) with cerebral atrophy preceding the involvement of cerebellar cortex; and *(c)* and an early cerebellar subtype (7.64% [21 of 275 participants]) showing cerebellar lobule atrophy before upper brainstem or cerebral involvement. More advanced disease stages (MRI-based SuStaIn stages) correlated with greater symptom duration (unstandardized coefficient $B = 0.422$, standard error = 0.065, $P < .001$) and severity ($B = 1.404$, standard error = 0.201, $P < .001$), and these relationships were moderated by subtype, with biologic stage progression in the early cerebral subtype mapping less strongly to clinical variables relative to the others (interaction term early cerebral subtype × stage: $B = -0.925$, standard error = 0.410, $P = .02$).

Conclusion: Using the SuStaIn algorithm, three distinct structural MRI–based subtypes of FRDA were identified, with different patterns of brain degeneration and associations with clinical severity.

Supplemental material is available for this article.

Friedreich ataxia (FRDA) is an inherited multisystem disease that includes progressive degeneration of the spinal cord, brainstem, cerebellum, and targeted regions of the cerebrum (1). MRI plays a crucial role in noninvasively characterizing disease-related brain changes and potentially providing biomarkers for patient stratification and treatment monitoring in clinical trials (2). Although the exact sequence of neuroanatomic changes occurring in the brain of individuals with FRDA is not definitely established, histologic and MRI studies have identified the above-mentioned brain regions as prominently involved in the neurodegenerative processes occurring in this condition and have provided insights into the evolution of the disease over time (3–6). On the other hand, there is substantial interindividual heterogeneity in the rate of progression and symptom profile of FRDA that remains poorly understood. This gap in knowledge, only partially explained by known genetic factors, such as GAA triplet-repeat expansion length in the *FXN* gene (7), highlights the need for novel imaging biomarkers that may enable more refined patient stratification. Indeed, as the drug development pipeline and initiation of clinical trials continue to expand, the need to meaningfully account for disease heterogeneity and stratify individuals with FRDA remains critical and is gaining urgency (8,9).

Quantitative MRI investigations of brain structure provide a viable approach to address this need. However, most MRI studies in individuals with FRDA to date have relied on small sample sizes, limiting the statistical power, the generalizability of the findings, and the ability to reliably model disease-related variability. The ENIGMA-Ataxia working group *(https://enigma.ini.usc.edu/*

Abbreviations

FRDA = Friedreich ataxia, SuStaIn = Subtype and Stage Inference

Summary

Using a machine learning approach, three distinct structural MRI–based biological subtypes of Friedreich ataxia were identified, with different patterns of brain degeneration and associations with clinical severity.

Key Results

- In this secondary analysis of 565 participants, the Subtype and Stage Inference (SuStaIn) algorithm was applied to brain MRI of participants with Friedreich ataxia and identified three subtypes: "classical" (66.5% [183 of 275 participants]), "early cerebral" (25.8% [71 of 275 participants]), and "early cerebellar" (7.64% [21 of 275 participants]).
- The classical subtype was characterized by an ascending gradient of damage from brainstem to cerebellar cortex to cerebrum, the early cerebral subtype was characterized by cerebral atrophy preceding the involvement of cerebellar cortex, and the early cerebellar subtype showed cerebellar lobule atrophy before upper brainstem or cerebral involvement.
- Advanced disease stages were associated with greater symptom duration ($B = 0.422$, $P < .001$) and severity ($B = 1.182$, $P < .001$).

ongoing/enigma-ataxia/) was formed to address this issue, opening new research opportunities by aggregating the data of patients with ataxias from multiple sites worldwide. The first study of the ENIGMA-Ataxia working group comparing patients with FRDA and healthy controls confirmed that volume loss in the brainstem, dentate nucleus, and cerebellar peduncles is a robust and early feature of the disease, followed by the involvement of the cerebral white matter, particularly in corticospinal pathways, with cerebellar and cerebral sensorimotor gray matter loss as later characteristics (3). However, participants in that study were stratified based on a coarse subgrouping relying on arbitrary cutoffs of onset age and symptom duration, and the possible existence of different groups exhibiting distinct trajectories of neurodegeneration progression was not considered (3). Indeed, FRDA is known to be phenotypically heterogeneous, with the interindividual variability possibly reflecting the existence of distinct latent disease subtypes and corresponding underlying pathophysiologic mechanisms (9). In this context, the recent development of machine learning algorithms in the field of data-driven disease progression modeling, combined with the increasing availability of large-scale neuroimaging datasets such as ENIGMA-Ataxia, offers new opportunities to objectively characterize the temporal and phenotypic heterogeneity of FRDA. In particular, the Subtype and Staging Inference (SuStaIn) algorithm (10) has emerged as a powerful solution to simultaneously model temporal and phenotypic heterogeneity in different neurologic conditions by inferring disease trajectories from cross-sectional data, without the need for multiple visits per patient (11–13).

This study aimed to obtain a structural MRI–based stratification of participants with FRDA using the SuStaIn algorithm and determine whether these subgroups are biologically meaningful and clinically relevant.

Materials and Methods

Study Sample

In this secondary analysis of prospectively acquired data, participants from the ENIGMA-Ataxia working group *(https://enigma.ini.usc.edu/ongoing/enigma-ataxia/)* were included. Written informed consent was obtained from each participant independently at each center, while multisite data aggregation and analysis were approved by the Monash University Human Research and Ethics Committee (project no. 12372).

Previously collected and analyzed T1-weighted MRI and clinical-demographic data of participants with FRDA and healthy participants of comparable age and sex (controls) from across 12 research centers were analyzed (3). Individuals with FRDA were genetically confirmed to have biallelic mutations in intron 1 of the *FXN* gene.

MRI Data Acquisition

The structural volumetric MRI data used in this study consisted of three-dimensional T1-weighted anatomic images obtained with 3-T or 1.5-T scanners with a voxel size of no greater than 1 mm^3 (Table S1). All participants from each center were scanned using the same MRI protocol, ensuring internal consistency within each site.

Image Processing

Details of the image processing pipeline are provided by Harding and colleagues (3). Briefly, images were processed with the Computational Anatomy Toolbox (CAT12 version 12.5; *https://neuro-jena.github.io/cat/*) for the quantification of cerebral gray matter and whole-brain white matter volumes and with the Spatially Unbiased Infratentorial Toolbox (SUIT version 3.2; *www.diedrichsenlab.org/imaging/suit.htm*) for cerebellar gray matter volume, using default settings. Preprocessing steps included segmentation into gray and white matter, normalization to standard space, and modulation by the Jacobian determinants derived during both linear and nonlinear spatial normalization to preserve volume encoding (15). Brain regions were defined according to the Harvard-Oxford cortical and subcortical atlases for cerebral gray matter, the Johns Hopkins University tractography atlas from the FMRIB Software Library (fsl.fmrib.ox.ac.uk, version 6.0) for cerebral white matter, the FreeSurfer subcortical atlas for the brainstem, the van Baarsen cerebellar white matter atlas for cerebellar peduncles (16), and the SUIT atlas for cerebellar gray matter lobules and dentate nuclei (17,18), for a total of 128 regions of interest. Regional volumes were calculated by multiplying the mean intensity of all voxels in the modulated tissue map (encoding local volume) within each region of interest by the total number of voxels in that region of interest. To eliminate nonbiological site-related variability, regional brain volumes were harmonized for center biases using ComBat (19,20) while preserving the variance associated with age, sex, and diagnosis (FRDA vs controls).

Clinical Evaluation

Disease severity was quantified using one of the following validated clinical scales: the Friedreich Ataxia Rating Scale (or FARS), the Scale for Assessment and Rating of Ataxia (or SARA), or the International Cooperative Ataxia Rating Scale (or ICARS), with higher scores indicating greater clinical severity. Disease severity measures for the different FRDA cohorts are reported in Table S2. To aggregate clinical scores across sites, we used the regression coefficients for scale interconversion provided by Rummey and colleagues (14), thus obtaining a single harmonized disease

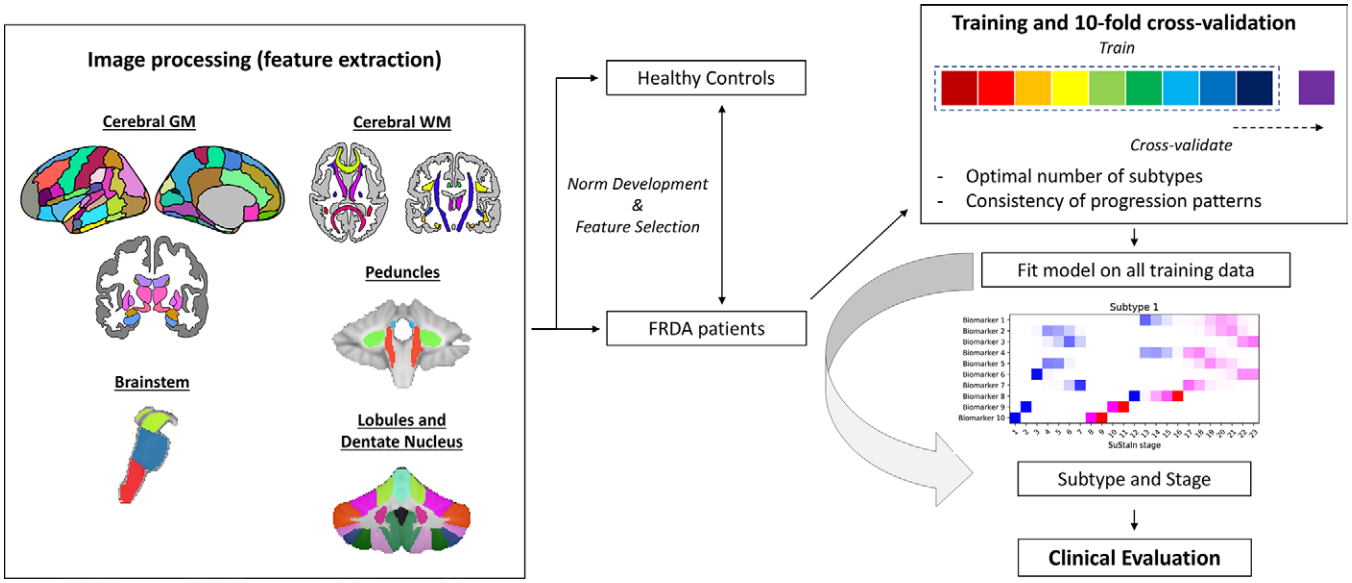

Figure 1: Outline of the main data processing and analysis steps. Structural MRI–derived brain volumes of participants with Friedreich ataxia (FRDA) are z-scored based on normative distributions in healthy controls and used as input for Subtype and Stage Inference (SuStaIn). Ten-fold cross-validation is conducted to determine the optimal number of subtypes and the consistency of progression patterns. GM = gray matter, WM = white matter.

severity score for all participants, expressed according to the FARS scale. Symptom duration was defined as the time elapsed between the onset of the first clinical symptoms attributable to the disease and the date of MRI.

Statistical Analysis

A flowchart summarizing the main data processing and analysis steps is depicted in Figure 1.

SuStaIn modeling

SuStaIn is an unsupervised machine learning algorithm (ie, capable of learning patterns from unlabeled data) that combines concepts from clustering and event-based modeling to infer data-driven subgroups characterized by common patterns of disease progression (subtypes) and individual severity (stages), even from purely cross-sectional data. In its most common implementation, disease progression is described as the linear evolution of biomarkers along discrete levels of cumulative alteration, defined in terms of deviation from a reference norm (z scores). Methodologic aspects of the SuStaIn algorithm are described in detail by Young and colleagues (10) and in the corresponding GitHub repository *(https://github.com/ucl-pond/pySuStaIn)*.

As SuStaIn can be computationally demanding for large numbers of biomarkers, and its performance depends on the balance between sample size and the number of biomarker events, we reduced dimensionality through a biologically informed feature selection procedure. First, data were summed across the equivalent regions in the left and right hemispheres to provide a single measure for each structure, supported by previous work indicating that brain atrophy is not likely lateralized in FRDA (3). Then, features that had at least a moderate between-group effect size (FRDA vs controls Cohen $d > 0.5$, adjusted for age, sex, and intracranial volume) were selected. The volume of each region was then converted to a z score with reference to the control group, adjusting for the physiologic effects of age, sex, and intracranial volume. Specifically, for each regional volume, a linear model with the confounders as independent variables was fit in the control group and used to generate predictions in participants with FRDA. Confounder-adjusted measures were obtained as the difference between raw and predicted values and standardized as follows: individual z score = (individual corrected value – mean of corrected values in the control group)/SD of corrected values in the control group (12). The signs of the z scores were flipped so that more positive values correspond to greater atrophy. To reduce computational complexity and ensure a balance between the number of biomarker events and sample size, analyses were focused on a single biomarker abnormality level, defined for a z score greater than 2 (10).

SuStaIn models with one, two, three, or four subtypes were trained and evaluated using 10-fold cross-validation. The number of subtypes that maximized the out-of-sample likelihood (and minimized the cross-validation Information Criterion) across cross-validation folds was considered to be optimal. The consistency of each subtype progression pattern across cross-validation folds (cross-validation similarity) was estimated with the Bhattacharyya coefficient, measuring the degree of overlap between two statistical samples (21). Finally, a model with the optimal number of subtypes was fitted to the whole dataset and used to obtain a probabilistic assignment of each participant with FRDA to a specific subtype and stage within a subtype. The assignment with the highest probability was used for further analyses.

Relationship between SuStaIn stratification and clinical features

To assess clinical-demographic correlates of the SuStaIn subtypes, we performed one-way analysis of variance (ANOVA) or χ^2 test analyses as appropriate to compare age, sex, onset age, symptom duration, disease severity, and length of the triplet repeat expansion in the *FXN* gene (shorter allele, GAA1), and site provenance between participants assigned to each subtype. Associations between SuStaIn stage and symptom duration and severity were also investigated using linear models controlling for age, age^2 (to account for the non-linear effect of age), and sex.

Table 1: Demographic and Clinical Characteristics of the Studied Participants

Participant and Study Location	No. of Participants	Sex*		Age (y)	Onset Age (y)	Symptom Duration (y)
		Female	Male			
FRDA						
Aachen	26	12 (46.2)	14 (53.8)	36 ± 12.2	16.7 ± 7.7	19.7 ± 9.6
Bologna	17	9 (52.9)	8 (47.1)	29 ± 12.8	8.9 ± 4.7	20.5 ± 11.4
Campinas	52	33 (63.5)	19 (35.5)	30 ± 13.6	18.2 ± 9.4	11.6 ± 9.2
Conegliano	39	20 (52.3)	19 (47.7)	23 ± 11.3	11.3 ± 7.1	11.6 ± 8.0
Essen	15	9 (60.0)	6 (40.0)	44 ± 11.3	21.4 ± 7.2	22.7 ± 8.4
Florence	17	9 (52.9)	8 (47.1)	32 ± 9.7	18.2 ± 9.0	14.2 ± 8.2
Innsbruck	13	6 (46.2)	7 (53.8)	46 ± 12.3	25.7 ± 12.2	20.3 ± 9.1
Melbourne I	31	14 (45.2)	17 (54.8)	37 ± 13.0	19.5 ± 8.8	17.0 ± 9.5
Melbourne II	13	4 (30.8)	9 (69.2)	29 ± 7.3	15.0 ± 4.0	13.5 ± 5.3
Minnesota	19	10 (52.6)	9 (47.4)	19 ± 7.4	13.8 ± 5.8	4.7 ± 3.1
Naples	19	6 (31.6)	13 (68.4)	28 ± 14.1	17.1 ± 9.9	11.6 ± 7.0
Tubingen	14	4 (28.6)	10 (71.4)	32 ± 11.4	17.7 ± 8.7	14.1 ± 6.9
All participants with FRDA	275	136 (49.5)	139 (50.5)	31 ± 13.6	16.6 ± 9.0	14.4 ± 9.5
Healthy controls	290	150 (51.7)	140 (48.3)	32 ± 12.6	NA	NA

Note.—Table shows characteristics of participants with Friedreich ataxia (FRDA) and healthy control participants across 12 study sites. Except where indicated, data are means ± SDs. NA = not applicable.

* Data are numbers of participants, with percentages in parentheses.

Additionally, to assess whether the relationship between stage and symptom severity and/or duration varied across subtypes, we tested the possible moderation effects of SuStaIn subtype by adding it and its interaction with stage to the models. Finally, we aimed to investigate the added value of the proposed data-driven staging in explaining clinical severity over an established MRI biomarker: using the Akaike Information Criterion and the likelihood ratio test, we evaluated the above-mentioned model against a baseline including demographic variables and the adjusted and standardized volume of the medulla, which has been previously reported as showing the greatest deviation from the healthy norm in this population (3). Statistical analyses were carried out using R (version 4.1.2), with a statistical significance level set at $P < .05$ (G.P.).

Results

Participant Characteristics

This study included 565 participants (mean age, 32 years ± 13.1 [SD]; 286 women; 275 participants with FRDA and 290 healthy controls) (Table 1).

SuStaIn Modeling Identifies Three Neurostructural Subtypes of Brain Degeneration in FRDA

The volumes of 21 brain regions survived the feature selection procedure, confirming established knowledge on this condition and including areas of the cerebral gray matter (precentral gyrus), white matter (cortico-spinal tract, anterior thalamic radiation, forceps major, superior longitudinal fasciculus, and inferior fronto-occipital fasciculus), the brainstem (midbrain, pons and medulla), cerebellar peduncles (inferior, superior, and middle), the dentate nucleus, and most cerebellar lobules (I–IV, X, VI, V, crus I, crus II, VIIb, IX) (Fig 2). The impact of ComBat harmonization on volume distributions is shown in Figure S1, while the effect sizes for all explored brain regions are provided in Figure S2.

The three-subtype model below was modestly superior to the two-subtype model, yielding the highest average log-likelihood (and lowest cross-validation Information Criterion) across cross-validation folds (Figs S3, S4). Each of the three subtypes was defined by distinct trajectories of brain atrophy progression (Fig 3). All three subtypes were characterized by initial volume loss in the ascending spinocerebellar tract (ie, inferior cerebellar peduncle), cerebello-cerebral tract (ie, superior cerebellar peduncle), and medulla. Thereafter, the progression patterns diverged according to a "classical" subtype (66.5% [183 of 275] of participants), where atrophy of the dentate nucleus, upper brainstem, cerebro-cerebellar pathway (ie, middle cerebellar peduncles), and corticospinal tracts was followed by the cerebellar lobules, the supratentorial association tracts, and, finally, the precentral gyrus; an "early cerebral" subtype (25.8% [71 of 275] of participants), whereby atrophy of the supratentorial association tracts and precentral gyrus preceded the involvement of the cerebellar lobules; and an "early cerebellar" subtype (7.7% [21 of 275] of participants), where cerebellar lobule atrophy preceded the involvement of the dentate nucleus and upper brainstem before progressing to the supratentorial association tracts and precentral gyrus.

Example images of participants with FRDA assigned to the three subtypes identified by SuStaIn are shown in Figure 4.

The progression patterns demonstrated high consistency across cross-validation folds, with mean cross-validation similarity of 0.98 ± 0.01, 0.96 ± 0.03, and 0.99 ± 0.01 for the classical, early cerebral, and early cerebellar subtypes, respectively (Fig S5).

Determining the optimal number of subtypes requires a careful balance between model complexity (ie, the number of subtypes), goodness-of-fit, and biologic plausibility and may involve a degree of arbitrariness. Consequently, the relatively simpler model with two subtypes is presented in Figure S6, which substantially corresponds to the classical and early cerebral subtypes.

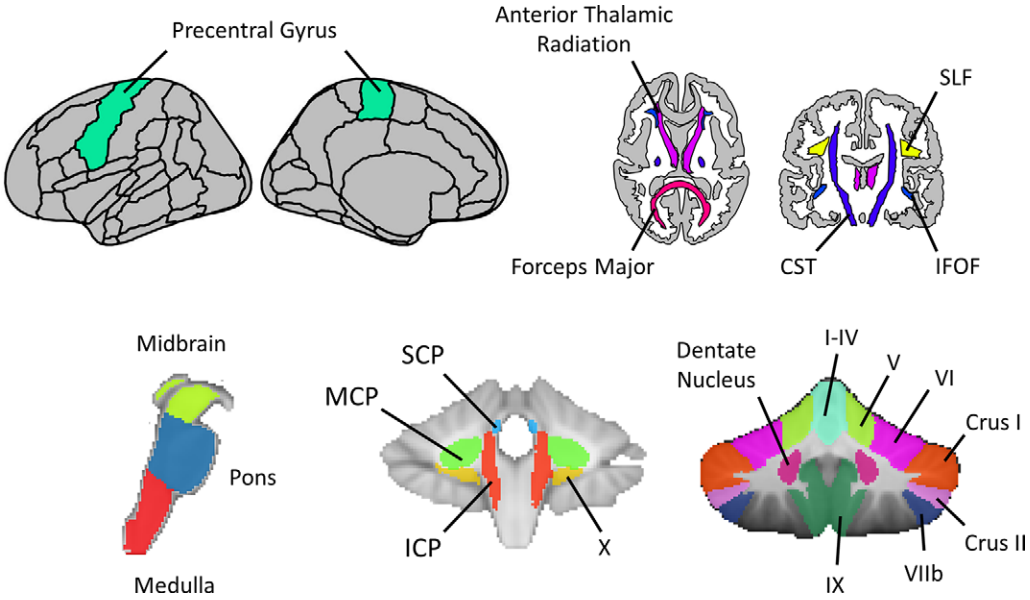

Figure 2: Diagram shows results of the feature selection procedure. Brain regions whose volume survived the feature selection procedure (ie, associated with a moderate to large effect size upon comparison with healthy controls) are presented, encompassing the cerebral gray matter (precentral gyrus) and white matter (cortico-spinal tract [CST], anterior thalamic radiation, forceps major, superior longitudinal fasciculus [SLF], and inferior fronto-occipital fasciculus [IFOF]), the brainstem (midbrain, pons, and medulla), cerebellar peduncles (inferior, superior, and middle), and the dentate nucleus and cerebellar lobules (I–IV, X, VI, V, crus I, crus II, VIIb, IX). ICP = inferior cerebellar peduncle, MCP = middle cerebellar peduncle, SCP = superior cerebellar peduncle.

Clinical Correlates of the MRI-based Stratification

There was no evidence of a difference between the three MRI-based subtypes in terms of sex, age, onset age, symptom duration, clinical severity, GAA triplet repeats (Table 2, Fig S7), or site provenance ($P = .84$, χ^2 test) (Fig S8). A difference in SuStaIn stage was evident between subtypes, with average biologic disease stage of the participants in each subgroup having progressively higher values going from the classical to the early cerebellar subtypes ($F[2, 272] = 3.72$, $P = .03$).

SuStaIn stage was associated with symptom duration (unstandardized coefficient $B = 0.422$, standard error = 0.065, $P < .001$), with greater disease duration corresponding to more advanced MRI disease stages. This is an expected effect, given that SuStaIn stages reflect the progression of atrophy patterns and provides a sanity check of the outcomes. Of greater interest, the strength of this relationship was moderated by SuStaIn subtype, with participants belonging to the classical ($B = 0.526$) and early cerebellar ($B = 0.279$) subtypes having a stronger association between MRI stage and symptom duration than those with the early cerebral subtype ($B = 0.159$) (interaction term early cerebral subtype × stage: $B = -0.381$, standard error = 0.161, $P = .02$) (Fig 5A, Table S3).

Similarly, MRI-based SuStaIn stage was also associated with disease severity as expressed by the harmonized Friedreich Ataxia Rating Scale ($B = 1.182$, standard error = 0.201, $P < .001$), with greater disease severity associated with more advanced MRI stage (Fig 5B, Table S4). Again, participants assigned to the early cerebral subtype exhibited a less steep positive relationship ($B = 0.540$) between stage and severity relative to those with classical ($B = 1.401$) and cerebellar cortex ($B = 0.905$) subtypes (interaction term early cerebral subtype × stage: $B = -0.925$, standard error = 0.410, $P = .02$) (Fig 5B, Table S4). When adjusting for demographic variables, SuStaIn stage explained clinical severity better (Akaike Information Criterion: 1939 vs 1945) and beyond ($P = .005$, likelihood ratio test) medullary atrophy (Table S5).

Finally, similar clinical correlates were observed for the two-subtype model (Figs S9–S11, Tables S6–S9).

Discussion

Using Subtype and Stage Inference (SuStaIn), we identified three distinct imaging-based subtypes of Friedreich ataxia, characterized by different trajectories of brain atrophy. This MRI-based stratification was both biologically plausible and clinically relevant, paving the way for future studies investigating both its potential as a novel tool for patient stratification in clinical and research settings and underlying disease mechanisms.

In most cases, participants with FRDA followed an "ascending" pattern of brain damage, from the medulla and inferior cerebellar peduncle to the cerebellum, to later involvement of the supratentorial compartment at the level of the motor cortex and major association tracts. We labeled this pattern the classical subtype, as it is consistent with the established neuropathology of FRDA, with the dorsal root ganglia and/or dorsal columns and the dentate nuclei recognized as primary sites of pathology, and transneuronal degeneration identified as a likely mechanism driving the spread of damage across the brain (22,23). Along with this classical subtype, we identified two additional MRI-based subtypes that we respectively defined as early cerebral and early cerebellar. While the involvement of supratentorial areas and the cerebellar cortex is a known feature of FRDA (5,24,25), atrophy of these regions is often reported as a late-stage phenomenon (3,26). The identification of subgroups in which these regions are impacted earlier in the disease course suggests that the SuStaIn algorithm is able to uncover minority subtypes that may have been obscured in previous group-level analyses. This result corroborates the importance of explicitly modeling intersubject heterogeneity to fully characterize and stratify cohorts of individuals with neurodegenerative diseases (10). Interestingly, atrophy of the cerebellar cortex tended to follow the same anteroposterior gradient in all three MRI subtypes, confirming the higher vulnerability to FRDA-related damage of the motor cerebellum compared with cerebellar areas associated with premotor and cognitive functions (3,27,28).

The question remains as to the source of the observed phenotypic heterogeneity and the possibility of different underlying pathophysiologic mechanisms. While the absence of more granular disease feature testing (ie, subscales) prevented us from assessing possible finer clinical correlates of the proposed stratification,

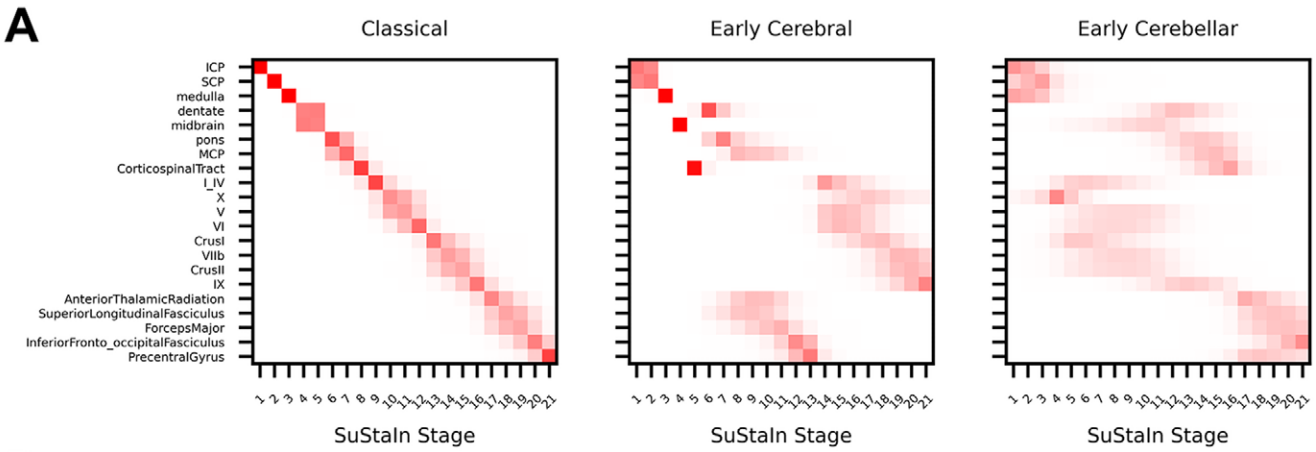

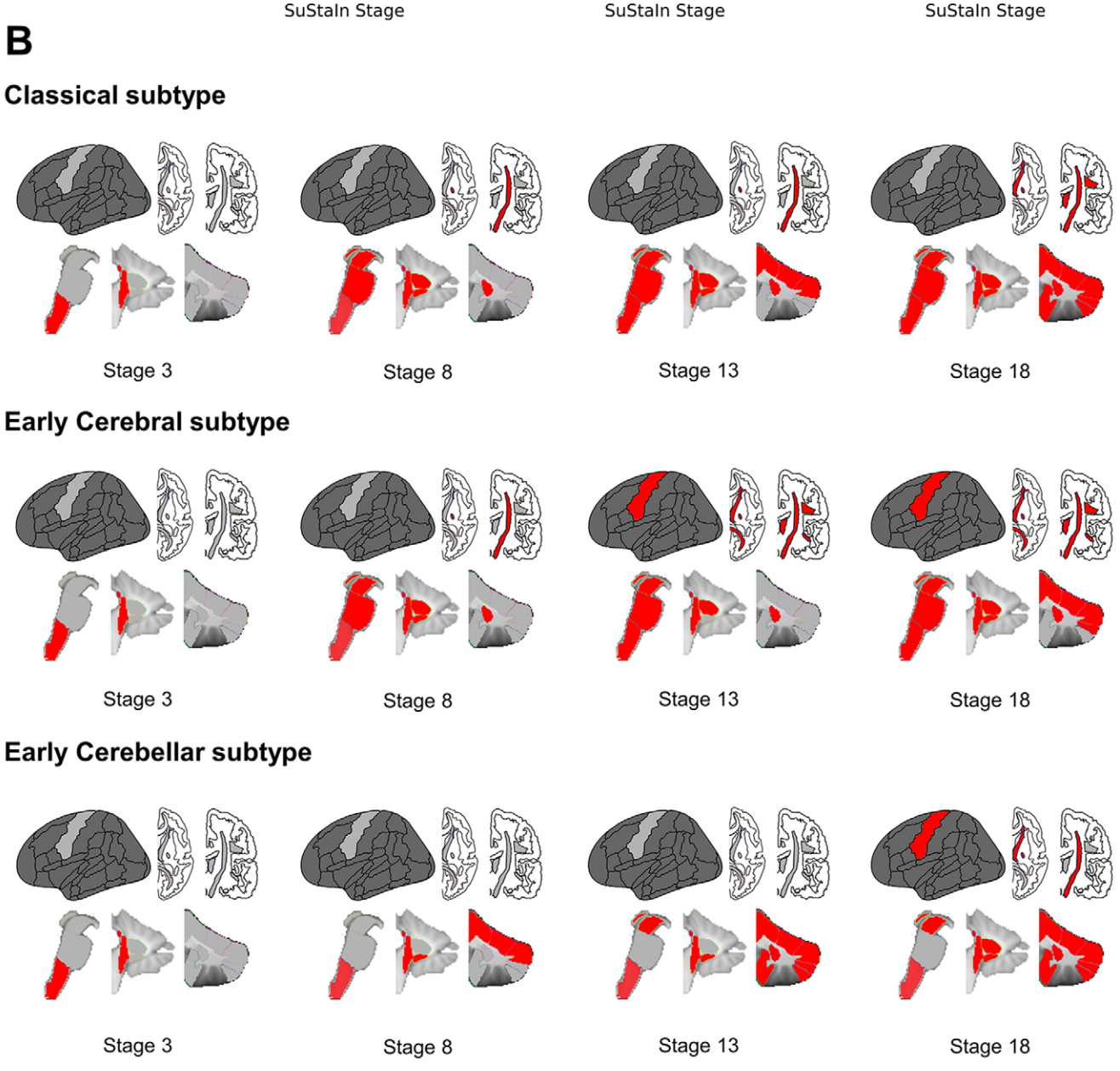

Figure 3: Representation of the three MRI-based subtypes. **(A)** Positional variance diagrams show the ordered sequence of abnormality events for the three MRI-based subtypes. Each entry describes the probability for each biomarker (y-axis) of becoming abnormal (ie, z score >2) at each Subtype and Stage Inference (SuStaIn) stage (x-axis). The color shade reflects the uncertainty (ie, the cumulative probability) associated with the corresponding biomarker event. **(B)** Graphical snapshots at stages 3, 8, 13, and 18 (chosen as representative examples uniformly sampling the progression trajectories) show the sequence of biomarker abnormalities for the three subtypes. Dark gray regions of interest are not included in the model. Selected regions of interest are shown in red or light gray according to whether the corresponding biomarkers have become abnormal at the presented stage. CST = cortico-spinal tract, ICP = inferior cerebellar peduncle, IFOF = inferior fronto-occipital fasciculus, MCP = middle cerebellar peduncle, SCP = superior cerebellar peduncle, SLF = superior longitudinal fasciculus.

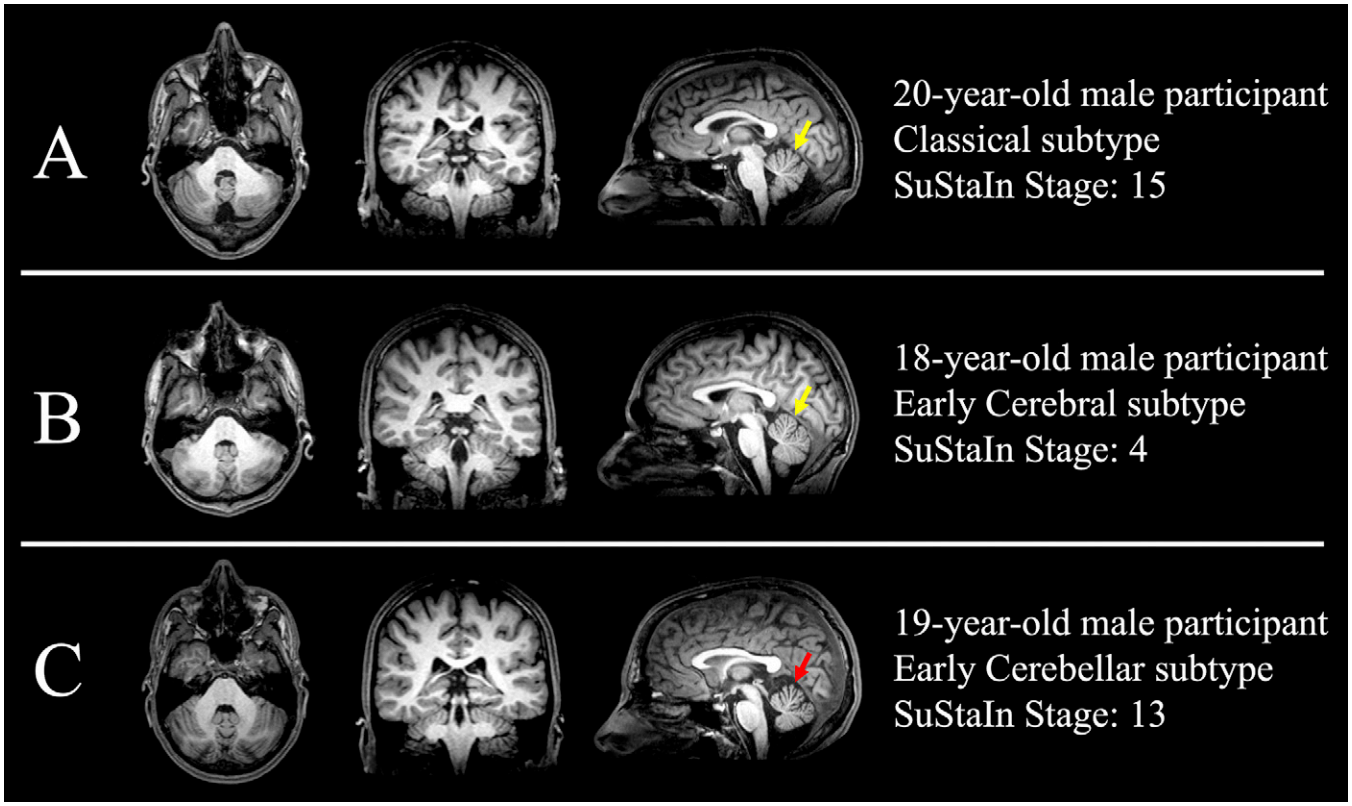

Figure 4: Example images in three patients with Friedreich ataxia (FRDA) assigned to different Subtype and Stage Inference (SuStaIn) subtypes. Multiplanar reconstructions (from left to right: axial, coronal, sagittal) from a three-dimensional T1-weighted sequence in three participants with FRDA selected to match site, sex, and age across subtypes. The three participants with FRDA were assigned to three different SuStaIn subtypes, but on conventional images they appear largely similar with only minor distinctions (eg, a slightly more pronounced cerebellar involvement in the early cerebellar subtype, indicated by the arrow in **C**, compared with the arrow in **A** and **B**), underscoring the added value of SuStaIn over visual analysis in capturing disease-related heterogeneity.

the MRI-based subtypes did not significantly differ in terms of clinical-demographic variables. This suggests that the subtyping was capturing latent disease "biotypes" rather than separating distinct demographic/clinical groups. However, the subgroups did not differ in terms of GAA1 triplet repeat length either, implying that the root of this disease-related variance might be non-genetic. Indeed, there are numerous reports of epigenetic heterogeneity among individuals with FRDA (29–34), which might be responsible, at least in part, for the observed interindividual variability. Further investigation of this interesting hypothesis is necessary.

When looking at the disease dynamics, higher MRI-based stages were associated with longer symptom duration and greater clinical severity, confirming that the proposed stratification is biologically meaningful and clinically relevant, as it captures the progressive nature of the disease and related disability. Interestingly, in participants with the early cerebral subtype, the slope of the associations between stage and duration and/or severity was significantly less steep relative to the other subtypes. Notably, this distinction occurs despite there being no significant differences in any demographic or clinical variable between subgroups. While these data-driven subtypes may not correspond to clearly separable clinical phenotypes, the observation that one of them is associated with a distinct clinical trajectory suggests that subtyping can reveal latent biologic heterogeneity that is not captured by traditional labels, uncovering clinically meaningful differences that would remain otherwise undetected. Furthermore, while the explanatory power of our data-driven stratification for measures of clinical status was relatively modest, this result is consistent with the known clinical-radiologic dissociation in FRDA, where conventional neuroimaging markers only partially reflect disease severity. In this light, the ability to account for approximately one quarter of the variance in clinical scores using MRI-derived subtype and stage, together with age and sex, supports the value of structural imaging as a clinically meaningful tool for patient stratification. Although it is not possible to draw definitive conclusions, compelling hypotheses emerge from this observation. Given the relative sparing of the cerebellar cortex until later in the disease course in this group, this finding may indicate that cerebellar cortical changes are key determinants or modifiers of ataxia progression, in addition or interaction with atrophy in "core" regions of pathology including the dentate nuclei and cerebellar peduncles. Indeed, volume loss in the cerebellar cortex is associated with increased clinical severity and poorer motor functions in individuals with FRDA (26,35,36), as well as greater disruption of large-scale brain network integrity and function (37–40). Taken together, integrity of the cerebellar cortex may be a key determinant of interindividual variability in the disease course.

Alternatively, these distinctions may reflect differential rates of change through the disease stages between subgroups. It is important to note that only the sequence, not the timescale, of biomarker abnormalities is estimated within the SuStaIn framework, meaning that the stages merely reflect the evolution of the spatial pattern of atrophy, but the average time to pass from one stage cannot be inferred and may vary across subtypes. Therefore,

Table 2: Demographic and Clinical Characteristics of Participants with FRDA according to MRI-based Subtype

Parameter	Classical Subtype	Early Cerebral Subtype	Early Cerebellar Subtype	*P* Value
No. of participants*	183 (66.5)	71 (25.8)	21 (7.6)	NA
Sex*				.26†
Female	91 (49.7)	38 (53.5)	7 (33.3)	
Male	92 (50.3)	33 (46.5)	14 (64.7)	
Age (y)	31.8 ± 13.2	29.0 ± 14.6	31.7 ± 13.9	.34‡
Onset age (y)	17.2 ± 8.9	14.9 ± 9.2	17.6 ± 8.5	.18‡
Symptom duration (y)	14.6 ± 9.4	14.1 ± 9.6	14.2 ± 10.5	.93‡
Harmonized FARS§	47.8 ± 16.6	49.1 ± 13.6	49.7 ± 21.2	.80‡
SuStaIn stage	5.7 ± 5.6	6.9 ± 4.9	8.8 ± 4.8	.03‡
GAA1 triplets‖	561.5 ± 209.9	598.0 ± 251.0	496.5 ± 237.4	.34‡
GAA2 triplets#	905.1 ± 184.1	795.1 ± 163.3	744.3 ± 255.0	.21‡

Note.—Participants assigned to the different subtypes were not significantly different in terms of demographic and clinical characteristics. Unless otherwise specified, data are means ± SDs. FARS = Friedreich's Ataxia Rating Scale, FRDA = Friedreich ataxia, NA = not applicable, SuStaIn = Subtype and Stage Inference.

* Data are numbers of participants, with percentages in parentheses.

† Determined with the χ^2 test.

‡ Determined with the one-way analysis of variance test.

§ Data are for 237 participants.

‖ There were 162 participants with this finding.

There were 33 participants with this finding.

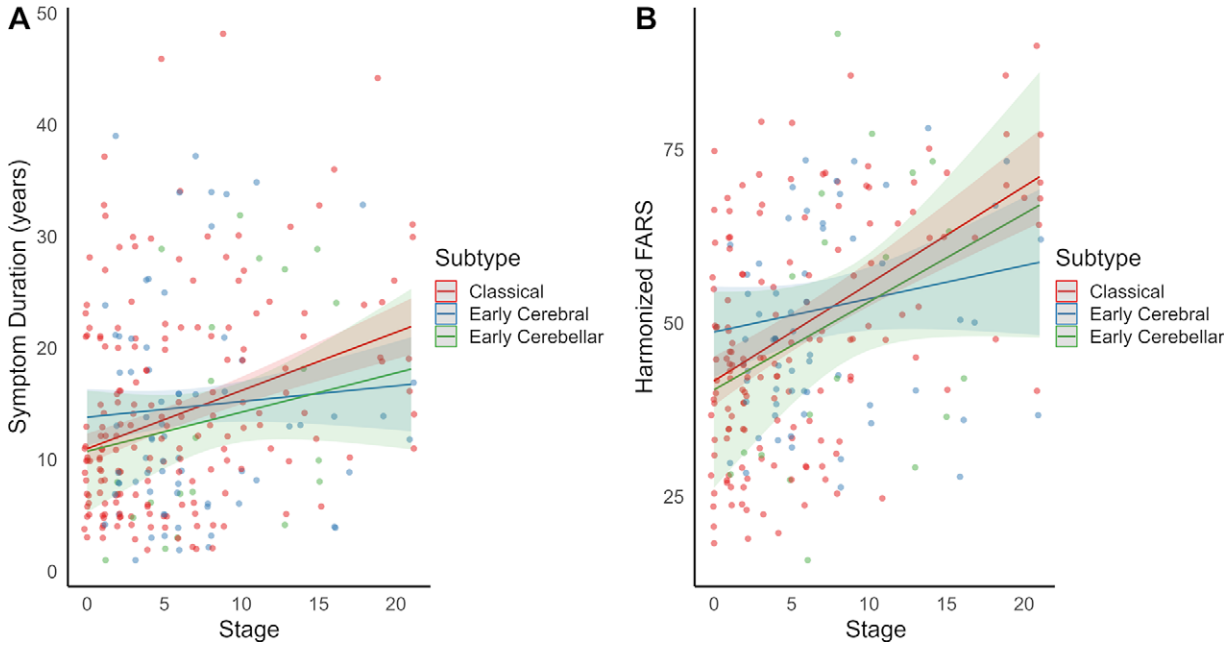

Figure 5: Relationships between MRI-based subtype, stage, and clinical variables. Interaction plots show how the marginal effects of Subtype and Stage Inference (SuStaIn) stage (x-axis) on **(A)** symptom duration and **(B)** disease severity vary across SuStaIn subtypes. Regression models were corrected for the effects of age, age^2, and sex. Each data point represents one participant. Linear fit lines are shown as solid lines with corresponding 95% CIs as shaded areas. FARS = Friedreich Ataxia Rating Scale.

a stronger linear relationship between symptom duration and biologic stage may reflect a more temporally consistent spatial progression, while greater temporal variability (eg, progressing quickly through some stages and slowly through others) would weaken this linear trend. The potential for these subtypes to have a different rate of biologic progression is an important hypothesis, requiring future follow-up with longitudinal data.

Several limitations were inherent to our study. First, the absence of follow-up examinations or the abovementioned lack of clinical subscales prevented us from evaluating our results longitudinally and assessing the prognostic value and the finer clinical correlates of the proposed stratification. In this regard, our study highlights the utility and power of a multisite data aggregation approach in this rare disease, but at the cost of limited availability of deeper clinical phenotypic measures. Future studies leveraging harmonized, prospective designs, such as TRACK-FA (41), will be critical to corroborate these patterns and clarify how data-driven subtypes may support patient

stratification in both diagnostic and therapeutic contexts. Furthermore, we only evaluated macroscopic regional brain volume obtained from T1-weighted MRI. Although this is the most widely accessible imaging modality in clinical and research settings, which maximizes translational opportunities, including information from additional MRI modalities (eg, tissue microstructure from diffusion-weighted imaging) might provide a more comprehensive characterization of FRDA-related brain damage. In addition, due to the need for data dimension reduction, we focused our analysis only on brain regions with the most prominent FRDA-related atrophy and neglected the possible contribution of neurodegeneration in more subtly affected brain regions (ie, frontal or parietal cortices) to interindividual variability in disease expression. Although we focused on the set of regions predominantly affected by FRDA, future work may explore other approaches encompassing, for example, feature aggregation, additional MRI modalities, or alternative disease progression modeling algorithms, to obtain a more comprehensive mapping of the brain. This could provide a broader picture of disease heterogeneity and help identify subtypes beyond those predominantly driven by well-established neuroanatomic alterations. Furthermore, in the preprocessing phase of the analysis workflow, we performed cross-site harmonization and, especially, feature selection on the entire dataset, a procedure that is susceptible to data leakage and might lead to overfitting of the models (42,43). However, feature selection was obtained by comparing patients to controls who were not included in the SuStaIn models, and results were fully consistent with those in the previous literature, suggesting that no new information derived from the entire dataset was introduced at this stage and making the risk of overfitting relatively limited. Finally, the lack of external testing may limit the cross-site generalizability of our findings, warranting replication in even larger and unseen FRDA cohorts when these become available.

In conclusion, using a machine learning approach that uses biologically informed feature selection and unsupervised disease progression modeling, three distinct MRI-based biologic subtypes of Friedreich ataxia (FRDA) were identified, each with different patterns of brain degeneration and associations with clinical severity. Nevertheless, further work is needed to elucidate the pathophysiologic mechanisms underlying the observed subtypes and to assess whether this stratification can support enrichment strategies for clinical trials, treatment monitoring, and, ultimately, personalized clinical management in FRDA.

Deputy Editor: Sven Haller
Scientific Editor: Kate Vilas

Author affiliations:

[1] Department of Advanced Biomedical Sciences, University Federico II, Via Pansini 5, 80131 Naples, Italy

[2] Department of Anatomy and Neurosciences, MS Center Amsterdam, Amsterdam Neuroscience, Amsterdam UMC, Vrije Universiteit Amsterdam, Amsterdam, the Netherlands

[3] Department of Radiology and Nuclear Medicine, MS Center Amsterdam, Amsterdam Neuroscience, Amsterdam UMC, Vrije Universiteit Amsterdam, Amsterdam, the Netherlands

[4] Queen Square Multiple Sclerosis Centre, Department of Neuroinflammation, UCL Queen Square Institute of Neurology, University College London, London, United Kingdom

[5] Enel Group, Sevilla, Spain

[6] Neuroimaging Unit, Scientific Institute, IRCCS Eugenio Medea, Bosisio Parini, Italy

[7] Department of Diagnostic and Interventional Neuroradiology, University Hospital Tübingen, Tübingen, Germany

[8] Department of Neurology, Medical University of Innsbruck, Innsbruck, Austria

[9] Department of Neurology, School of Medical Sciences, University of Campinas (UNICAMP), Campinas, SP, Brazil

[10] Brazilian Institute of Neuroscience and Neurotechnology (BRAINN), School of Medical Sciences, University of Campinas (UNICAMP), Campinas, SP, Brazil

[11] Centre for Youth Mental Health, The University of Melbourne, Melbourne, Australia

[12] Bruce Lefroy Centre, Murdoch Children's Research Institute, Parkville, VIC, Australia

[13] Department of Paediatrics, University of Melbourne, Parkville, VIC, Australia

[14] University Clinic and Outpatient Clinic for Radiology, Department for Radiation Medicine, University Hospital Halle (Saale), University Medicine Halle, Halle (Saale), Germany

[15] Victorian Clinical Genetics Services, Parkville, VIC, Australia

[16] Department of Electrical, Electronic, and Information Engineering Guglielmo Marconi, University of Bologna, Bologna, Italy

[17] Department of Neurology, RWTH Aachen University, Aachen, Germany

[18] JARA-BRAIN Institute Molecular Neuroscience and Neuroimaging, Research Center Jülich GmbH, Jülich, Germany

[19] Monash Biomedical Imaging, Monash University, Melbourne, Australia

[20] Turner Institute for Brain and Mental Health & School of Psychological Sciences, Monash University, Clayton, VIC, Australia

[21] Institute of Diagnostic and Interventional Radiology and Neuroradiology and Center for Translational Neuro- and Behavioral Sciences (C-TNBS), Essen University Hospital, University of Duisburg-Essen, Essen, Germany

[22] Center for Magnetic Resonance Research, Department of Radiology, University of Minnesota, Minneapolis, Minn

[23] Faculty of Computer Science, Dalhousie University, Halifax, Canada

[24] Department of Biomedical and Neuromotor Sciences, University of Bologna, Bologna, Italy

[25] Functional and Molecular Neuroimaging Unit, IRCCS Institute of Neurological Sciences of Bologna, Bologna, Italy

[26] Department for Life Quality Sciences, University of Bologna, Bologna, Italy

[27] Scientific Institute, IRCCS Eugenio Medea, Conegliano-Pieve di Soligo Research Centre, Conegliano, Italy

[28] Department of Statistics, Computer Science, and Applications Giuseppe Parenti, University of Florence, Florence, Italy

[29] Department of Clinical and Experimental Biomedical Sciences Mario Serio, University of Florence, Florence, Italy

[30] Department of Neurosciences and Reproductive and Odontostomatological Sciences, University of Naples Federico II, Naples, Italy

[31] GENESIS Department, University of Naples Federico II, Naples, Italy

[32] Department of Neurodegenerative Diseases, Hertie Institute for Clinical Brain Research, Tübingen, Germany

[33] German Center for Neurodegenerative Diseases (DZNE), Tübingen, Germany

[34] Imaging Genetics Center, Mark and Mary Stevens Institute for Neuroimaging and Informatics, Keck School of Medicine, University of Southern California, Marina del Rey, Calif

[35] Department of Neurology and Center for Translational Neuro- and Behavioral Sciences (C-TNBS), Essen University Hospital, University of Duisburg-Essen, Essen, Germany

[36] Child and Adolescent Neuropsychiatry Unit, Department of Women's and Children's Health, Padua University Hospital, Padua, Italy

[37] QIMR Berghofer Medical Research Institute, Brisbane, Australia

[38] School of Translational Medicine, Monash University, Melbourne, Australia

Received May 9, 2025; revision requested June 17; final revision received December 19; accepted January 26, 2026.

Address correspondence to: S.C. (email: sirio.cocozza@unina.it).

Supplemental material: Supplemental material is available at *Radiology* online.

Funding: This work was partly supported by the following research grants: Italian Ministry of Health (RF 2011-02437420); Italian Ministry of Research, under the

complementary actions to the NRRP "Fit4MedRob - Fit for Medical Robotics" grant (no. PNC0000007); Christina Foundation; Interdisciplinary Center for Clinical Research within the faculty of Medicine at the RWTH Aachen University, Germany (OC2); FARA (Friedreich's Ataxia Research Alliance, grant 92133) and FAPESP (São Paulo Research Foundation) through CEPID/BRAINN (grant 2013/07559-3); German Research Foundation (DFG, DE 2516/1-1 and TI 239/17-1); Australian National Health and Medical Research Council (ideas grant 1184403; investigator grant 2026191), Friedreich Ataxia Research Alliance; Friedreich Ataxia Research Alliance (FARA) with additional support from Ataxia UK, Go Friedreich's Ataxia Research (GoFAR), the CureFA Foundation and the Bob Allison Ataxia Research Center (BAARC); National Institutes of Health (NIH) grants P41EB027061, P30NS076408, and S10OD017974; Deutsche Forschungsgemeinschaft (DFG, German Research Foundation, no. 4414096270); Australian National Health and Medical Research Council (ideas grant 1184403; investigator grant 2026191); NIH Big Data to Knowledge (BD2K) award (U54 EB020403); and NIH grants (R01MH123163, R01MH121246, and R01MH116147). For a complete list of ENIGMA-related grant support please see here: *http://enigma.ini.usc.edu/about-2/funding/*.

Acknowledgments: The authors thank Christoph Scherfler, MD, and Stefania Tirelli, MSc, for their assistance in data acquisition at their centers.

Author contributions: Giuseppe Pontillo: Conceptualization, Data curation, Formal analysis, Software, Writing - original draft; Simone Penna: Data curation, Formal analysis, Software, Validation, Writing - original draft; Filippo Arrigoni: Data curation, Investigation, Writing - review & editing; Benjamin Bender: Data curation, Investigation, Writing - review & editing; Sylvia Boesch: Data curation, Investigation, Writing - review & editing; Arturo Brunetti: Data curation, Investigation, Writing - review & editing; Fernando Cendes: Data curation, Investigation, Writing - review & editing; Sidhant Chopra: Data curation, Investigation, Writing - review & editing; Louise A Corben: Data curation, Investigation, Writing - review & editing; Andreas Deistung: Data curation, Investigation, Writing - review & editing; Martin B Delatycki: Data curation, Investigation, Writing - review & editing; Stefano Diciotti: Data curation, Investigation, Writing - review & editing; Imis Dogan: Data curation, Investigation, Writing - review & editing; Gary Egan: Data curation, Investigation, Writing - review & editing; Marcondes C França Junior: Data curation, Investigation, Writing - review & editing; Nellie Georgiou-Karistianis: Data curation, Investigation, Writing - review & editing; Sophia Luise Goericke: Data curation, Investigation, Writing - review & editing; Pierre-Gilles Henry: Data curation, Investigation, Writing - review & editing; Carlos R. Hernandez-Castillo: Data curation, Investigation, Writing - review & editing; Diane Hutter: Data curation, Investigation, Writing - review & editing; James M Joers: Data curation, Investigation, Writing - review & editing; Christophe Lenglet: Data curation, Investigation, Writing - review & editing; Tobias Lindig: Data curation, Investigation, Writing - review & editing; Raffaele Lodi: Data curation, Investigation, Writing - review & editing; David Neil Manners: Data curation, Investigation, Writing - review & editing; Alberto R. M. Martinez: Data curation, Investigation, Writing - review & editing; Andrea Martinuzzi: Data curation, Investigation, Writing - review & editing; Chiara Marzi: Data curation, Investigation, Writing - review & editing; Mario Mascalchi: Data curation, Investigation, Writing - review & editing; Wolfgang Nachbauer: Data curation, Investigation, Writing - review & editing; Chiara Pane: Data curation, Investigation, Writing - review & editing; Denis Peruzzo: Data curation, Investigation, Writing - review & editing; Pramod K Pishardy: Data curation, Investigation, Writing - review & editing; Kathrin Reetz: Data curation, Investigation, Writing - review & editing; Thiago Rezende: Data curation, Investigation, Writing - review & editing; Sandro Romanzetti: Data curation, Investigation, Writing - review & editing; Francesco Saccà: Data curation, Investigation, Writing - review & editing; Ludger Schöls: Data curation, Investigation, Writing - review & editing; Jörg B Schulz: Data curation, Investigation, Writing - review & editing; Ambra Stefani: Data curation, Investigation, Writing - review & editing; Matthis Synofzik: Data curation, Investigation, Writing - review & editing; Sophia I Thomopoulos: Funding acquisition, Resources, Writing - review & editing; Paul Thompson: Funding acquisition, Resources, Writing - review & editing; Dagmar Timmann: Data curation, Investigation, Writing - review & editing; Caterina Tonon: Data curation, Investigation, Writing - review & editing; Marinela Vavla: Data curation, Investigation, Writing - review & editing; and Ian H Harding: Conceptualization, Funding acquisition, Project administration, Supervision, Writing - review & editing; Sirio Cocozza: Conceptualization, Data curation, Project administration, Supervision, Visualization, Writing - original draft, Writing - review & editing.

Disclosures of conflicts of interest: Please see ICMJE form(s) for author conflicts of interest. These have been provided as supplemental materials.

References

1. Campuzano V, Montermini L, Moltò MD, et al. Friedreich's Ataxia: Autosomal Recessive Disease Caused by an Intronic GAA Triplet Repeat Expansion. Science 1996;271(5254):1423–1427.
2. Öz G, Cocozza S, Henry PG, et al; AGI Working Group on MRI Biomarkers. MR Imaging in Ataxias: Consensus Recommendations by the Ataxia Global Initiative Working Group on MRI Biomarkers. Cerebellum 2024;23(3):931–945. [Published correction appears in Cerebellum 2024;23(3):946–947.]
3. Harding IH, Chopra S, Arrigoni F, et al. Brain Structure and Degeneration Staging in Friedreich Ataxia: Magnetic Resonance Imaging Volumetrics from the ENIGMA-Ataxia Working Group. Ann Neurol 2021;90(4):570–583.
4. Rezende TJR, Adanyeguh IM, Arrigoni F, et al. Progressive Spinal Cord Degeneration in Friedreich's Ataxia: Results from ENIGMA-Ataxia. Mov Disord 2023;38(1):45–56.
5. Adanyeguh IM, Joers JM, Deelchand DK, et al. Brain MRI detects early-stage alterations and disease progression in Friedreich ataxia. Brain Commun 2023;5(4):fcad196.
6. Joers JM, Adanyeguh IM, Deelchand DK, et al. Spinal cord magnetic resonance imaging and spectroscopy detect early-stage alterations and disease progression in Friedreich ataxia. Brain Commun 2022;4(5):fcac246.
7. Bidichandani SI, Delatycki MB, Napierala M, Duquette A. Friedreich Ataxia. In: Adam MP, Bick S, Mirzaa GM, et al, eds. GeneReviews®. University of Washington, 1993.
8. U.S. Food & Drug Administration. FDA approves first treatment for Friedreich's ataxia. https://www.fda.gov/drugs/news-events-human-drugs/fda-approves-first-treatment-friedreichs-ataxia. Accessed February 28, 2023.
9. Rummey C, Corben LA, Delatycki M, et al. Natural History of Friedreich Ataxia: Heterogeneity of Neurologic Progression and Consequences for Clinical Trial Design. Neurology 2022;99(14):e1499–e1510.
10. Young AL, Marinescu RV, Oxtoby NP, et al; Alzheimer's Disease Neuroimaging Initiative (ADNI). Uncovering the heterogeneity and temporal complexity of neurodegenerative diseases with Subtype and Stage Inference. Nat Commun 2018;9(1):4273.
11. Oxtoby NP. Data-Driven Disease Progression Modeling. In: Colliot O, ed. Machine Learning for Brain Disorders. Vol 197. Springer, 2023; 511–532. doi:10.1007/978-1-0716-3195-9_17.
12. Eshaghi A, Young AL, Wijeratne PA, et al. Identifying multiple sclerosis subtypes using unsupervised machine learning and MRI data. Nat Commun 2021;12(1):2078. [Published correction appears in Nat Commun 2021;12(1):3169.]
13. Vogel JW, Young AL, Oxtoby NP, et al; the Alzheimer's Disease Neuroimaging Initiative. Four distinct trajectories of tau deposition identified in Alzheimer's disease. Nat Med 2021;27(5):871–881.
14. Rummey C, Harding IH, Delatycki MB, et al. Harmonizing results of ataxia rating scales: mFARS, SARA, and ICARS. Ann Clin Transl Neurol 2022;9(12):2041–2046.
15. Ashburner J, Friston KJ. Voxel-Based Morphometry—The Methods. Neuroimage 2000;11(6 Pt 1):805–821.
16. van Baarsen KM, Kleinnijenhuis M, Jbabdi S, et al. A probabilistic atlas of the cerebellar white matter. Neuroimage 2016;124(Pt A):724–732.
17. Diedrichsen J, Balsters JH, Flavell J, Cussans E, Ramnani N. A probabilistic MR atlas of the human cerebellum. Neuroimage 2009;46(1):39–46.
18. Diedrichsen J, Maderwald S, Küper M, et al. Imaging the deep cerebellar nuclei: A probabilistic atlas and normalization procedure. Neuroimage 2011;54(3):1786–1794.
19. Johnson WE, Li C, Rabinovic A. Adjusting batch effects in microarray expression data using empirical Bayes methods. Biostatistics 2007;8(1):118–127.
20. Fortin JP, Cullen N, Sheline YI, et al. Harmonization of cortical thickness measurements across scanners and sites. Neuroimage 2018;167:104–120.
21. Bhattacharyya AK. On a Measure of Divergence between Two Multinomial Populations. Sankhya Ind J Stat 1933-1960 1946;7(4):401–406. https://www.jstor.org/stable/25047882.
22. Koeppen AH, Mazurkiewicz JE. Friedreich Ataxia: Neuropathology Revised. J Neuropathol Exp Neurol 2013;72(2):78–90.
23. Harding IH, Lynch DR, Koeppen AH, Pandolfo M. Central Nervous System Therapeutic Targets in Friedreich Ataxia. Hum Gene Ther 2020;31(23-24):1226–1236.
24. Selvadurai LP, Corben LA, Delatycki MB, et al. Multiple mechanisms underpin cerebral and cerebellar white matter deficits in Friedreich ataxia: The IMAGE-FRDA study. Hum Brain Mapp 2020;41(7):1920–1933.
25. Oppenheimer DR. Brain Lesions in Friedreich's Ataxia. Can J Neurol Sci 1979;6(2):173–176.
26. Selvadurai LP, Harding IH, Corben LA, et al. Cerebral and cerebellar grey matter atrophy in Friedreich ataxia: the IMAGE-FRDA study. J Neurol 2016;263(11):2215–2223.
27. Stoodley CJ, Schmahmann JD. Functional topography in the human cerebellum: A meta-analysis of neuroimaging studies. Neuroimage 2009;44(2):489–501.
28. Stoodley CJ, Schmahmann JD. Evidence for topographic organization in the cerebellum of motor control versus cognitive and affective processing. Cortex 2010;46(7):831–844.
29. Rodden LN, Gilliam KM, Lam C, Lynch DR, Bidichandani SI. Epigenetic Heterogeneity in Friedreich Ataxia Underlies Variable FXN Reactivation. Front Neurosci 2021;15:752921.

30. Rodden LN, Chutake YK, Gilliam K, et al. Methylated and unmethylated epialleles support variegated epigenetic silencing in Friedreich ataxia. Hum Mol Genet 2021;29(23):3818–3829.
31. Rodden LN, Rummey C, Dong YN, Lynch DR. Clinical Evidence for Variegated Silencing in Patients With Friedreich Ataxia. Neurol Genet 2022;8(3):e683.
32. Lam C, Gilliam KM, Rodden LN, et al. *FXN* gene methylation determines carrier status in Friedreich ataxia. J Med Genet 2023;60(8):797–800.
33. Castaldo I, Pinelli M, Monticelli A, et al. DNA methylation in intron 1 of the frataxin gene is related to GAA repeat length and age of onset in Friedreich ataxia patients. J Med Genet 2008;45(12):808–812.
34. Reetz K, Dogan I, Costa AS, et al. Biological and clinical characteristics of the European Friedreich's Ataxia Consortium for Translational Studies (EFACTS) cohort: a cross-sectional analysis of baseline data. Lancet Neurol 2015;14(2):174–182.
35. Della Nave R, Ginestroni A, Giannelli M, et al. Brain structural damage in Friedreich's ataxia. J Neurol Neurosurg Psychiatry 2008;79(1):82–85.
36. França MC, D'Abreu A, Yasuda CL, et al. A combined voxel-based morphometry and 1H-MRS study in patients with Friedreich's ataxia. J Neurol 2009;256(7):1114–1120.
37. Harding IH, Corben LA, Delatycki MB, et al. Cerebral compensation during motor function in Friedreich ataxia: The IMAGE-FRDA study. Mov Disord 2017;32(8):1221–1229.
38. Harding IH, Corben LA, Storey E, et al. Fronto-cerebellar dysfunction and dysconnectivity underlying cognition in friedreich ataxia: The IMAGE-FRDA study. Hum Brain Mapp 2016;37(1):338–350.
39. Cocozza S, Costabile T, Tedeschi E, et al. Cognitive and functional connectivity alterations in Friedreich's ataxia. Ann Clin Transl Neurol 2018;5(6):677–686.
40. Kerestes R, Cummins H, Georgiou-Karistianis N, et al. Reduced cerebellocerebral functional connectivity correlates with disease severity and impaired white matter integrity in Friedreich ataxia. J Neurol 2023;270(5):2360–2369.
41. Georgiou-Karistianis N, Corben LA, Reetz K, et al. A natural history study to track brain and spinal cord changes in individuals with Friedreich's ataxia: TRACK-FA study protocol. PLoS One 2022;17(11):e0269649. [Published corrections appear in PLoS One 2025;20(3):e0320683 and PLoS One 2025;20(5):e0324751.]
42. Marzi C, Giannelli M, Barucci A, et al. Efficacy of MRI data harmonization in the age of machine learning: a multicenter study across 36 datasets. Sci Data 2024;11(1):115.
43. Rosenblatt M, Tejavibulya L, Jiang R, Noble S, Scheinost D. Data leakage inflates prediction performance in connectome-based machine learning models. Nat Commun 2024;15(1):1829.